Title

Modifying Li+ and Anion Diffusivities in Polyacetal Electrolytes: A Pulsed-Field-Gradient NMR Study of Ion Self-Diffusion

Journal

Chemistry of Materials, 33(13)

ISSN

0897-4756

Authors

Halat, David M
Snyder, Rachel L
Sundararaman, Siddharth
et al.

Publication Date

2021-07-13

DOI

10.1021/acs.chemmater.1c00339

Peer reviewed

Modifying Li^+ and Anion Diffusivity in Polyacetal Electrolytes: A PFG-NMR Study of Ion Self-Diffusion

David M. Halat,[1,2,3,†] Rachel L. Snyder,[2,4,†] Siddharth Sundararaman,[2,5] Youngwoo Choo,[2,3] Kevin W. Gao,[1,2,3] Zach J. Hoffman,[1,2,3] Brooks A. Abel,[2,4] Lorena S. Grundy,[1,2,3] Michael D. Galluzzo,[1,2,3] Madeleine P. Gordon,[5,6] Hasan Celik,[1] Jeffrey J. Urban,[5] David Prendergast,[2,5] Geoffrey W. Coates,*[,2,4] Nitash P. Balsara,*[,1,2,3] and Jeffrey A. Reimer*[,1,2,3]

[1] Department of Chemical and Biomolecular Engineering and College of Chemistry, University of California, Berkeley, California 94720, United States

[2] Joint Center for Energy Storage Research, Argonne National Laboratory, Lemont, Illinois 60439, United States

[3] Materials Sciences Division, Lawrence Berkeley National Laboratory, Berkeley, California 94720, United States

[4] Department of Chemistry and Chemical Biology, Baker Laboratory, Cornell University, Ithaca, New York 14853, United States

[5] The Molecular Foundry, Lawrence Berkeley National Laboratory, Berkeley, California 94720, United States

[6] Applied Science and Technology Graduate Group, University of California, Berkeley, California 94720, United States

KEYWORDS. Electrolytes, Polymers, Lithium-ion, Diffusion, Polyacetals, Ions, Transport properties, NMR

ABSTRACT: Polyacetal electrolytes have been demonstrated as promising alternatives to liquid electrolytes and PEO for rechargeable lithium-ion batteries; however, the relationship between polymer structure and ion motion is difficult to characterize. Here, we study structure–property trends in ion diffusion with respect to polymer composition for a systematic series of five polyacetals with varying ratios of ethylene oxide (EO) to methylene oxide (MO) units, denoted P(*x*EO-*y*MO), and PEO. We first use ^{7}Li and ^{19}F pulsed-field-gradient NMR spectroscopy to measure cation and anion self-diffusion, respectively, in polymer/lithium bis(trifluoromethanesulfonyl)imide (LiTFSI) salt mixtures. At 90 °C, we observe modest changes in Li^+ diffusivity across all polymer compositions while anion ($TFSI^-$) self-diffusion coefficients decrease significantly with increasing MO content. At a given reduced temperature ($T - T_g$), all polyacetal electrolytes exhibit faster Li^+ self-diffusion than PEO. Intriguingly, P(EO-MO) and P(EO-2MO) also show slower $TFSI^-$ anion self-diffusion than PEO at a given reduced temperature. Molecular dynamics simulations reveal that shorter distances between acetal oxygen atoms ($O–CH_2–O$) compared to ether oxygens ($O–CH_2–CH_2–O$) promote more diverse, often asymmetric, Li^+ coordination environments. Raman spectra reveal that anion-rich ion clusters in P(EO-MO) and P(EO-2MO) lead to decreased anion diffusivity, which along with increased cation diffusivity, elucidate the viability of polyacetals as high-performance polymer electrolytes.

Introduction

The revolution in personal mobile electronics[1] and push towards using lithium-ion batteries (LIBs) for transportation and grid-scale energy storage[2–4] has ignited a renewed interest in polymer electrolytes, which can be used in place of flammable liquid electrolytes[5,6] to mitigate safety concerns and improve compatibility with high-capacity Li metal anodes. Although many polymer electrolytes have been studied,[7] poly(ethylene oxide) (PEO) mixed with a lithium salt has remained the most promising polymer electrolyte since the early studies of Fenton, Parker, and Wright[8] and Armand.[9] In practice, however, slow ion transport in polymer electrolytes prevents sufficient Li-ion conductivity for adequate device performance at operational temperatures.[10–12] In PEO, for example, ions are transported by hopping and/or shuttling between solvation sites made up of Lewis-basic oxygens in a mechanism that is facilitated by segmental motion of the polymer chains.[13] The high concentration of oxygens in PEO readily solvate Li^+ salts, forming stable single-chain helical configurations around the cations.[14,15] However, these stable binding motifs significantly restrict movement of electrochemically active Li^+.[10–12] In contrast, the anions in PEO electrolytes do not coordinate strongly to the polymer backbone,[16–18] leading to undesirably low cationic transference numbers unsuitable for high-rate electrochemical applications.[19]

An outstanding goal of polymer electrolyte development is to improve overall ion mobility by selecting host structures that improve Li^+ transport and/or enhance Li^+ motion relative to anion motion.[19,20] Candidate polymer electrolytes must have well-connected solvation sites and good segmental motion of the polymer at operational

temperatures (i.e., low glass transition temperatures, T_g). Some systems are also designed to selectively enhance lithium motion relative to motion by promoting anion–polymer interactions.[20,21]A variety of discrete polymer functionalities that alter cation mobility,[22–26] improve segmental motion,[27,28] or suppress anion mobility[29] have been developed, but to date have not matched ion transport observed in PEO.

Working within these guidelines, another design strategy is to replace ethylene oxide (EO) repeat units (O–CH_2–CH_2) with acetals, i.e., methylene oxide (MO) repeat units (O–CH_2), to form polyacetals. Polyacetals maintain desirably high oxygen to carbon ratios, yet structural differences can decrease the strong intrachain crown-ether-like cation binding geometries found in PEO,[30] potentially facilitating improved cation mobility. Several polyacetals have shown promise as electrolytes in Li-ion batteries.[31–40] Our groups recently reported trends in conductivity (κ) and cationic current fraction (ρ_+) with polymer composition for a full series of five polyacetals and PEO at a range of LiTFSI concentrations.[41] This systematic approach revealed trends with respect to oxygen to carbon ratio (p = [O] / [C]) at a given salt concentration (r = 0.08). While κ values decreased approximately four times with increasing p, ρ_+ values increased nearly five-fold with increasing p. By calculating the efficacy (defined as $\kappa \times \rho_+$) of each polymer electrolyte composition, we identified that poly(1,3-dioxolane) (P(EO-MO)) and poly(1,3,5-trioxepane) (P(EO-2MO)) have higher efficacies than PEO at high and low salt concentrations, respectively.

Overall ion transport is dictated by both ion mobility and diffusivity. While ion mobility is difficult to independently characterize, ionic diffusivity can be studied in the absence of an electric potential using pulsed-field-gradient nuclear magnetic resonance spectroscopy (PFG-NMR), also referred to as pulsed-gradient spin–echo (PGSE) NMR. This affords a direct, spectroscopically-specific probe of cation or anion self-diffusion in polymer electrolytes[42] and provides discrete information about both cation and anion diffusivity that is often unavailable by electrochemical measurements.[17,43–46]

In the present work, we use a combination of spectroscopic measurements and molecular dynamics simulations to understand how underlying ion–polymer interactions influence ion diffusivity in polyacetals. Using PFG-NMR, we observe that Li^+ self-diffusion at a fixed temperature (90 °C) changes only minimally as a function of p, whereas $TFSI^-$ self-diffusion decreases dramatically with increasing acetal content. Because the polymer compositions exhibit significantly different glass transition temperatures (T_g), we consider ion self-diffusion at reduced temperature ($T - T_g$). We find that all polyacetals show increased Li^+ self-diffusion as compared to PEO at a given reduced temperature. P(EO-MO) and P(EO-2MO), the two compositions previously found to have the highest efficacy, also demonstrate considerably slower $TFSI^-$ self-diffusion than PEO at a given reduced temperature. Molecular dynamics (MD) simulations of P(EO-MO) reveal additional acetal oxygens in proximity to Li^+, which appear to improve cation hopping and/or shuttling. Furthermore, as anticipated, asymmetric Li^+ coordination environments within P(EO-MO) are observed. Finally, Raman spectra reveal signatures of anion clustering in P(EO-MO) and P(EO-2MO). Overall, these results provide a fundamental understanding of ion binding and clustering effects that result in the observed trends in κ and ρ_+ and ultimately provide high efficacy in P(EO-MO) and P(EO-2MO) polymer electrolytes.

Results and Discussion

Polymer Synthesis and Characterization. Polyacetals have been actively studied for over 80 years and are commonly synthesized via cationic ring-opening polymerization (CROP) of strained cyclic acetal monomers using a Brønsted or Lewis acid catalyst.[47–49] The polymers studied in this work are identical to our previous report.[41] We selected our cyclic acetal monomer scope in order to incrementally vary the ratio of EO to MO units in the resultant polymers (Scheme 1). In the following discussion, we consider the materials according to their oxygen-to-carbon ratio, p (Figure 1a), ranging from p = 0.50 for PEO (no acetals) to p = 0.75 for P(EO-2MO) (most acetal-rich).

Cyclic acetal monomers 1,3,6,9,12-pentaoxacyclotetradecane (4EO-MO), 1,3,6,9-tetraoxacycloundecane (3EO-MO), and 1,3,6-trioxocane (2EO-MO) were synthesized using a previously reported method.[39,50,51] These reactions were performed on a large scale (>30 g), wherein a given diol and paraformaldehyde were first step-growth polymerized in the presence of catalytic non-volatile polyphosphoric acid, followed by depolymerization of the oligomeric product at high temperatures to give the desired cyclic acetal. 1,3-Dioxolane (EO-MO) was purchased commercially, and insertion of formaldehyde into EO-MO in the presence of an acid catalyst yielded 1,3,5-trioxepane (EO-2MO).[52] Detailed synthetic procedures are described in the Supporting Information (SI §1–4).

Traditionally in CROP of cyclic acetals, acid catalysts react with nucleophilic acetal oxygens to form propagating oxonium or oxocarbenium species.[53] In this work, methyltriflate (MeOTf) or trimethylsilyltriflate (TMSOTf) was used as the acid-producing catalyst, reacting with trace water in the reaction mixture to generate triflic acid (Scheme 1).[54] Because the concentration of acid initiator is dependent on an unknown concentration of trace H_2O, it is difficult to control for polymer molecular weight across multiple batches of material.[55] Therefore, we tuned monomer concentration and equivalents of MeOTf or TMSOTf to obtain comparable molecular weights (M_n = 13.6–24.9 kDa) for poly(1,3,6,9-tetraoxacycloundecane) (P(3EO-MO)), poly(1,3,6-trioxocane) (P(2EO-MO)), poly(1,3-dioxolane) (P(EO-MO)), and poly(1,3,5-trioxepane) (P(EO-2MO)) (Table S1). Poly(1,3,6,9,12-pentaoxacyclotetradecane) (P(4EO-MO)) reached a molar mass of only 5.2 kDa, likely because low ring-strain in 14-membered 4EO-MO prevents high conversion.[50,51,56] The polymers were obtained in moderate yields (56–70%), and all data match previous reports of P(4EO-MO),[50,51,56] P(3EO-MO),[50,51,56–58] P(2EO-MO),[39,40,59,60] P(EO-MO),[54] and P(EO-2MO).[61]

Typically, polyacetals exhibit poor thermal stability, presumably because residual acidic species catalyze ring-closing depolymerization at elevated temperatures.[33] To

improve thermal stability, we employed an alkoxide quenching agent, sodium 2-trimethylsilylethoxide (NaOEtTMS), which is readily soluble in hexanes and ether and is easily removed during polymer precipitation (Scheme 1). Dynamic thermogravimetric analysis (TGA) shows excellent thermal stability with decomposition temperatures (i.e., observation of >5% weight loss) above 266 °C for all polymer compositions, well above temperatures considered in this study (Figure S7).

All polymers show unimodal molecular weight distributions by gel permeation chromatography (GPC) with no observable low molecular weight macrocyclic byproducts (Figure S1). ^{1}H NMR spectra of the purified polymers confirmed regioselective CROP of 4EO-MO, 3EO-MO, 2EO-MO, and EO-MO with a single acetal resonance indicating regioregular EO/MO sequences (SI §8). The ^{1}H NMR spectrum of P(EO-2MO) shows the polymer retains a 1:2 ratio of EO/MO units but reveals three distinct acetal resonances in a 1:2:1 ratio. Subsequent ^{13}C and HSQC NMR experiments identify the acetal resonances as (1) EO-**MO**-EO, (2) EO-**MO**-MO or MO-**MO**-EO, and (3) MO-**MO**-MO sequences in the polymer backbone, similar to previous reports.[61] Differential scanning calorimetry (DSC) demonstrates that all neat polymer compositions have similar T_g values (−62 to −66 °C); however, melting temperatures (T_m = 20–58 °C) and semi-crystalline behavior vary significantly with polymer composition (Figures S2–S6). Notably, P(3EO-MO)

Scheme 1. Typical Reaction Conditions and Monomer Scope for the Cationic Ring-Opening Polymerization of Cyclic Acetals to Polyacetals.

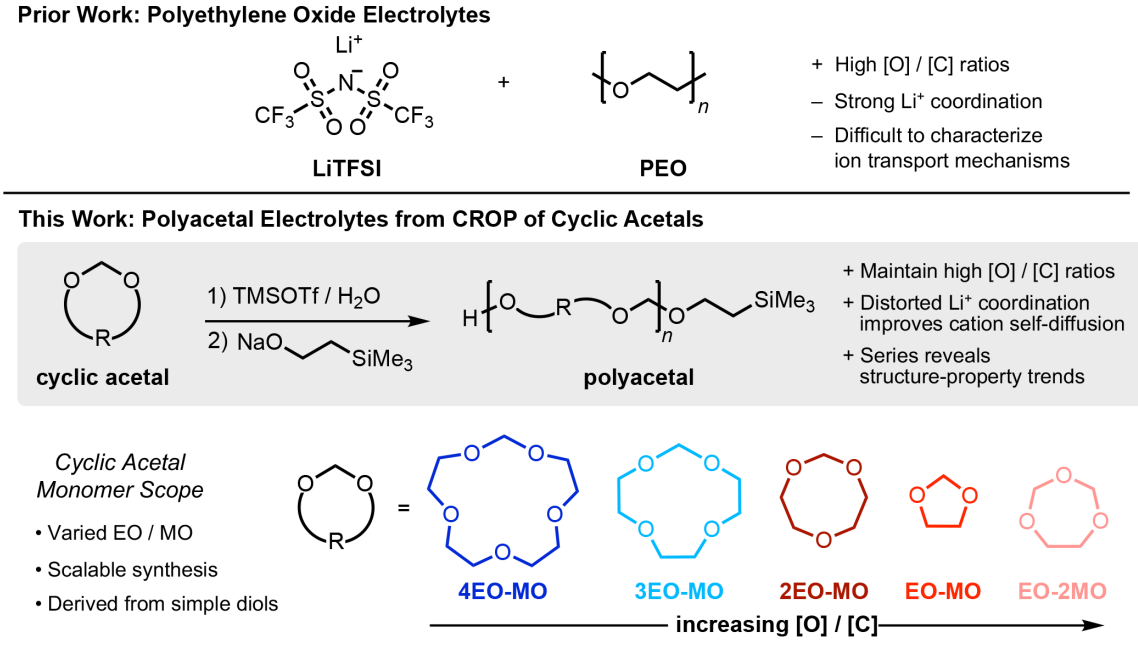

is amorphous (Figure S3), whereas P(4EO-MO) exhibits unique crystallization behavior during the second heating step (Figure S2). A summary of the physical properties of the synthesized polyacetal materials as well as PEO is given in Table S1.

Polymer electrolytes were prepared from the five purified polymers P(4EO-MO), P(3EO-MO), P(2EO-MO), P(EO-MO), and P(EO-2MO) by dissolving the polymer and LiTFSI salt in acetonitrile, mixing, evaporating the solvent, and drying the samples extensively under vacuum at elevated temperatures (see Supporting Information for detailed procedures). In PEO and other polyacetal electrolytes, the salt concentration is typically defined as the ratio of lithium cations to oxygen atoms in the polymer (r = [Li$^+$] / [O]).[39] In our polyacetal series, the concentration of oxygen changes with polymer composition, resulting in slightly different absolute salt loadings (variance ≤ 5.6 wt% LiTFSI) for each polyacetal at a given r value (Table S2). As the overall change in [LiTFSI] is relatively small, we chose to follow the conventional definition of salt loading in order to normalize [Li$^+$] to the number of available oxygen binding groups in our systems. The observed trends with respect to wt% LiTFSI are reported in the Supporting Information. Samples were prepared with loadings of r = 0.03 – 0.10, similar to previous studies of PEO and P(2EO-MO).[19,39]

Pulsed-field-gradient (PFG) NMR Measurements. We performed ^{7}Li and ^{19}F PFG-NMR measurements at 90 °C to unambiguously measure self-diffusion coefficients of the cation (Li$^+$) and anion (TFSI$^-$), respectively. The solid polyacetal/LiTFSI electrolyte mixtures were loaded into NMR tubes at elevated temperature and sealed under an argon atmosphere. In PEO, ion diffusivity and transport are quite slow at room temperature; as a result, measurements are often performed at elevated temperatures.[17,39,40,43] We performed measurements at 90 °C in order to compare with our previously published electrochemistry data.[41] Samples were measured after a temperature equilibration period of 20–30 minutes. We selected a 13-interval stimulated-echo pulse sequence[65] (Figure S10), which has been shown to mitigate artifacts arising from internal magnetic field gradients in solid and semi-solid samples.[66,67] In general, signal attenuation curves as a function of gradient strength show excellent agreement with fits to the modified Stejskal-Tanner equation (Figures S11 and S14). Self-diffusion

coefficients did not vary appreciably with diffusion time (Figure S12), suggesting that restricted diffusion effects were insignificant (see SI §10–11).

Cation and anion self-diffusion coefficients (D_{Li} and D_F) at 90 °C were compared at a given salt concentration defined as r (Figures 1b and 1c, respectively; Tables S3–S4) or wt% LiTFSI (Figures S18 and S19, respectively). Identical trends are observed when defining the salt concentration by either r = [Li]/[O] or wt% LiTFSI, suggesting the trends are related to polymer structure rather than absolute salt loading. The remaining discussion will focus on salt concentrations as quantified by r = [Li]/[O]. Data for PEO are taken from previous reports using similar methods.[62–64] Two different molecular weights of PEO (5 kDa and 20 kDa) are considered in order to reflect the full molar mass range of the polyacetals (5.6 kDa–26.1 kDa; Table S1), though variations in ^{7}Li and ^{19}F self-diffusion coefficients as a function of M_n are known to be minimal in this range.[62]

We first considered trends in both cation and anion diffusivity with respect to salt concentration (Figures 1b and 1c). Similar to prior studies of PEO,[62,68] both D_{Li} and D_F for each polymer decrease by a factor of two to three across the range of concentrations (r = 0.03–0.10). This trend is typically attributed to non-covalent

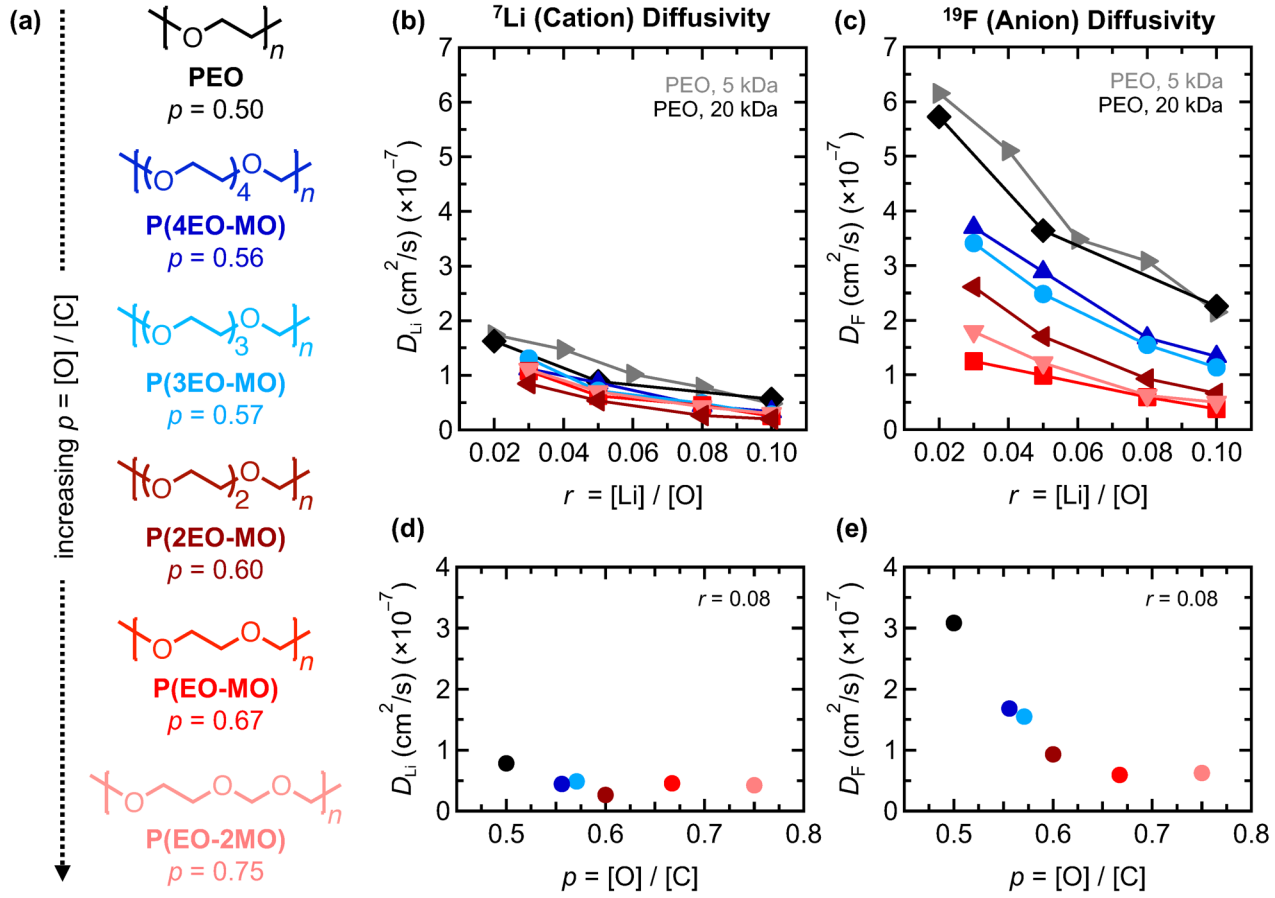

Figure 1. (a) Structures of PEO and the polyacetal series with increasing oxygen-to-carbon ratios (p = [O] / [C]). (b) Li^+ (^{7}Li) and (c) $TFSI^-$ (^{19}F) self-diffusion coefficients measured using PFG-NMR at 90 °C across a range of salt concentrations (r = [Li] / [O]); the color scheme follows (a). For all samples, Li^+ and $TFSI^-$ self-diffusion coefficients decrease with increasing salt concentration. (d) Li^+ (^{7}Li) and (e) $TFSI^-$ (^{19}F) self-diffusion coefficients compared as a function of p at r = 0.08. While Li^+ self-diffusion shows minimal variation with polymer composition, $TFSI^-$ self-diffusion decreases significantly with increasing acetal content. Self-diffusion coefficients for PEO are taken from previously reported experimental values[62] (5 kDa) or a combination of experimental and interpolated values[62–64] (20 kDa), the latter calculated using the reported power-law fit.[62] (Cation and anion self-diffusion coefficients are plotted with the same scale for direct comparison; for an expanded view of the cation data, see Figure S15.)

"cross-linking" of the polymer chains by Li^+ cations, leading to slowing down of both polymer and ion dynamics. We observed several intriguing trends in both cation and anion diffusivities with increasing acetal content (p) of the polymer host (Figures 1d and 1e). While D_{Li} decreases only slightly across the polymer series, D_F decreases significantly from PEO to P(EO-2MO). Figures 1d and 1e depict cation and anion diffusivities at a single salt concentration (r = 0.08) for all polymers. As p increases, an almost six-fold decrease in the anion self-diffusion coefficient occurs, with a less than two-fold change in the cation diffusivity (also see Figure S15b). Similar trends are observed across all r values.

The cationic contribution to diffusivity in the polyacetal samples is given via the PFG-NMR cationic transference number,[62,69]

$$t_+^{PFG} = \frac{D_{Li}}{D_{Li} + D_F} \quad (1)$$

which provides a qualitative comparison to the cationic transference numbers measured by electrochemical methods;[70–72] these two values should not be expected to agree quantitatively except for in ideal dilute systems.[72–78] The t_+^{PFG} values are averaged across all salt concentrations for each composition (Figure 2; Table S5). Temperature dependence of t_+^{PFG} appears minimal (Figure S20). As a function of p, a modest increase is initially observed, followed by a dramatic uptick to $t_+^{PFG} \approx 0.4$ for P(EO-MO) and P(EO-2MO). These two acetal-rich systems thus possess a greater relative cationic contribution to diffusivity. A comparison of t_+^{PFG} values with our previously reported[41] electrochemical current fraction (ρ_+) values (for $r = 0.08$) determined by the Bruce-Vincent method[79,80] shows excellent agreement in trends. There is thus a direct connection between self-diffusion coefficients of the ions and electrochemical properties of the electrolyte (*vide infra*).

Ion transport is also well-known to be coupled to segmental dynamics,[81,82] as reflected by T_g. As such, it is critical to decouple the ion–polymer and segmental motion effects in these systems in order to understand their individual effects on the observed ionic diffusivity. To quantify segmental motion, we measured the T_g values of each polymer at $r = 0.08$ using DSC (Figure S8); the T_g value for PEO was taken from the literature.[39,83] For all polymers, a substantial increase in T_g is observed when LiTFSI is added (Figure 3). The T_g values increase most dramatically for polymers with greater acetal content, i.e., P(2EO-MO), P(EO-MO), and P(EO-2MO). The T_g value of P(2EO-MO) at $r = 0.08$ is nearly 30 °C higher than that of PEO at $r = 0.08$, while P(EO-MO) and P(EO-2MO) have T_g values almost 20 °C higher than PEO at the same salt concentrations. This significant divergence in the salt-rich materials is also expected to impact the ion self-diffusion coefficients.[84,85] PFG-NMR

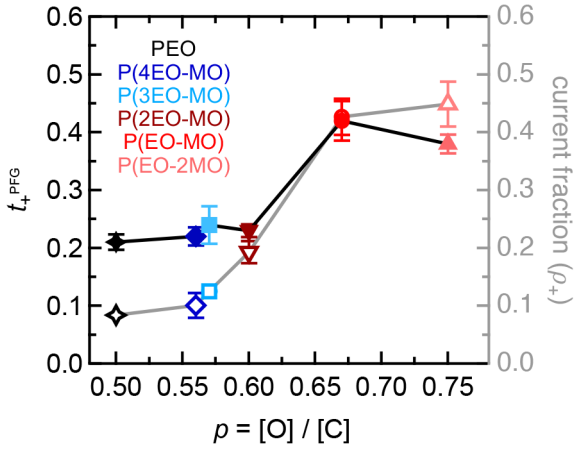

Figure 2. Comparison of PFG-based cationic transference numbers, t_+^{PFG}, averaged across all salt concentrations measured in this work (black line; filled symbols) and current fraction values at $r = 0.08$ measured in the previous report[41] (grey line; unfilled symbols). Both measurements show larger values with increasing p, reaching a plateau with P(EO-MO) and P(EO-2MO). Diffusion coefficients were measured at 90 °C. The t_+^{PFG} values are averaged across all studied salt concentrations and error bars indicate the standard deviation across the range of salt concentrations. The t_+^{PFG} value for PEO ($M_n = 5$ kDa) was calculated using self-diffusion coefficients from the prior literature.[39,62–64] The lines are included as a visual guide.

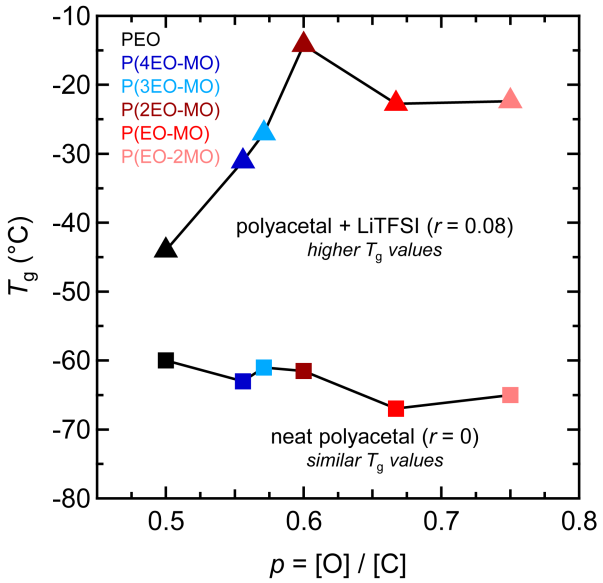

Figure 3. Glass transition temperatures (T_g) of the neat polymers ($r = 0$, ■) and of the electrolytes at a single salt concentration ($r = 0.08$, ▲) across the polymer series as measured by DSC. While neat polymers show similar, relatively low T_g values, the presence of LiTFSI dramatically increases the T_g as p increases, eventually reaching a plateau with P(EO-MO) and P(EO-2MO). T_g values for PEO are taken from the previous literature.[39,83]

measurements were done at a single temperature of 90 °C, which reflects a wide range of temperatures relative to T_g, and therefore, significant variation in segmental dynamics. To account for these differences, self-diffusion coefficients were considered as a function of the reduced temperature,[44] $T - T_g$, for both D_{Li} and D_F at $r = 0.08$ (Figure 4). Zheng *et al.* previously reported ion diffusivity in PEO/LiTFSI ($r = 0.08$) at multiple temperatures,[39] which we use here to directly compare PEO to each polyacetal at the same reduced temperature.

Each polyacetal demonstrates Li^+ self-diffusion coefficients higher than the interpolated values for PEO at a given reduced temperature (Figure 4a). This increase in D_{Li} relative to PEO is smallest for P(4EO-MO) and P(3EO-MO). The most acetal-rich polymers P(2EO-MO), P(EO-MO), and P(EO-2MO) have D_{Li} values twice that of PEO at the same reduced temperature. This enhanced Li^+ diffusivity is presumably driven by favorable changes in the cation–polymer interactions (see **MD Simulations** below). As a result, cation diffusivity varies negligibly when measured at 90 °C (Figure 1d), as the increasing diffusivity from improved cation–polymer interactions counteracts the effects of slowed segmental motion. While cation diffusivity in all polyacetals exceeds that of PEO, anion diffusivity in P(4EO-MO), P(3EO-MO), and P(2EO-MO) is comparable to PEO at their respective reduced temperatures (Figure 4b). Therefore, the observed decrease in D_F at 90 °C can be attributed to changes in segmental dynamics for these three systems. By contrast, the most acetal-rich systems P(EO-MO) and P(EO-2MO) exhibit D_F values nearly two times lower than that of PEO at

the same reduced temperature. Consequently, both segmental motion and additional underlying factors such as anion–polymer interactions and/or ion clustering may play a role in the decreased anion diffusivity at 90 °C (Figure 1e). Factoring out the effect of segmental motion reveals that the polyacetal composition modulates both cationic *and* anionic phenomena.

Molecular Dynamics Simulations. We next probed the molecular origins for the observed differences in ion self-diffusion using molecular dynamics (MD) simulations. Specifically, we focus on atomic features that could cause faster cation diffusivity and/or slower anion diffusivity in the most acetal-rich polyacetals. We constructed, annealed, and simulated PEO/LiTFSI and a representative polyacetal electrolyte P(EO-MO)/LiTFSI at r = 0.08. The effective temperature for all simulations was 363 K (90 °C); see SI §13 for further methodological details. We initially hypothesized that cation diffusivity would be influenced by both cation–polymer and cation–anion interactions. First, we studied the local Li^+ solvation structures in both PEO and P(EO-MO). Representative snapshots from MD simulations of these systems are depicted in Figure 5a. As expected and previously observed,[81,86] the first coordination shell of Li^+ in the PEO system consists of six polymer oxygens arranged in an octahedral-like geometry with four oxygen atoms in-plane and two axial oxygen atoms (Figure 5a, left). Notably in PEO, all oxygens near Li^+ are located within 3 Å, and no significant differences exist between the two coordination structures at cut-off distances of 3 Å and 4 Å. In P(EO-MO), however, representative snapshots reveal significantly distorted geometries (Figure 5a, right). In particular, the shortened oxygen–oxygen distances in acetals appear to discourage the helical intrachain configurations around Li^+ that promote a stable octahedral geometry. Yamashita and coworkers have reported a similar experimental result regarding Na^+ and K^+ uptake and coordination in macrocyclic acetals versus crown ethers.[30]

In addition to distorted binding motifs, P(EO-MO) snapshots reveal a second Li^+ coordination shell between 3 and 4 Å, meaning that additional oxygens are in close proximity to Li^+ (Figure 5a, bottom right). The snapshots in Figure 5a are statistically corroborated by Li–$O_{polymer}$ radial distribution function (RDF) bond distance curves (Figure 5b). While the RDF data are similar for PEO and P(EO-MO) up to 3 Å, a secondary peak for P(EO-MO) is present,

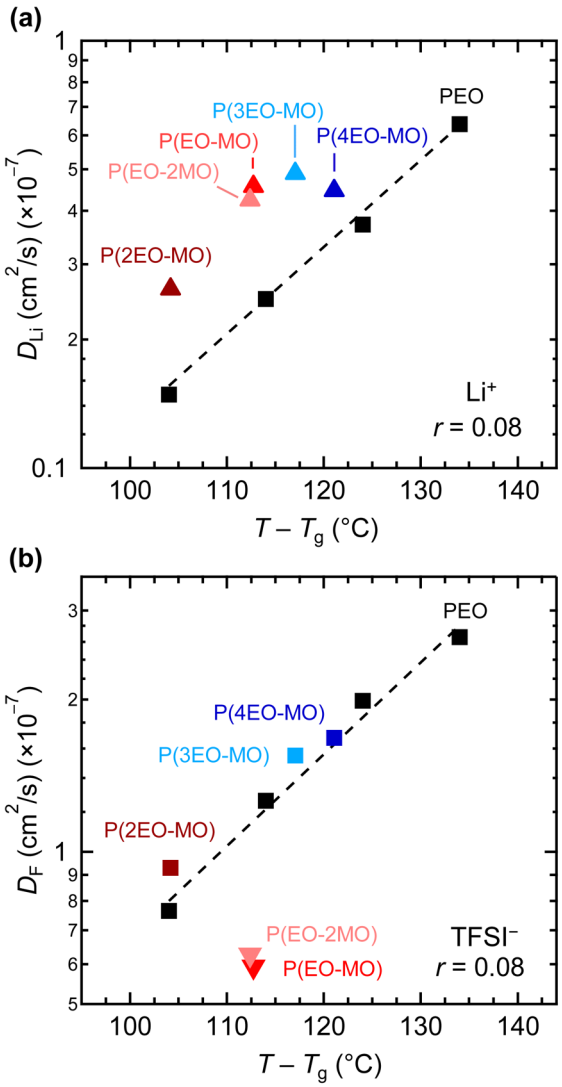

Figure 4. (a) Li^+ (^{7}Li) and (b) $TFSI^-$ (^{19}F) self-diffusion coefficients for each polyacetal at a single salt concentration (r = 0.08), compared to the self-diffusion of PEO (■) as a function of reduced temperature ($T - T_g$). Self-diffusion coefficients for PEO were previously measured at 60, 70, 80, and 90 °C.[39,62–64] At a given reduced temperature, Li^+ self-diffusion is faster in all polyacetal compositions as compared to PEO. In most cases, $TFSI^-$ self-diffusion is comparable to PEO, except for P(EO-MO) and P(EO-2MO) which show reduced D_F at equivalent reduced temperature. The T_g values shown in Figure 3 were used to calculate the reduced temperatures. Error bars are smaller than the marker size.

corresponding to a second coordination shell between 3 and 4 Å (inset). Combining these two observations, it is apparent that, on average, Li^+ in P(EO-MO) resides in distorted environments as compared to the symmetrical binding motifs in PEO, and oxygens in the second coordination shell are readily available to facilitate movement of Li^+ from one solvation structure to another.[87]

To obtain insight into the degree of cation–anion clustering and/or aggregation, we calculated RDF distance curves between Li^+ and $TFSI^-$ oxygens (Figure 5c). The distinct peak at 2 Å corresponds to Li^+ cations in close proximity to $TFSI^-$ and is representative of contact ion pairs or

cation–anion clusters. P(EO-MO) has a smaller degree of pairing interactions as evidenced by the weaker intensity of the 2 Å peak relative to PEO. From this result, we conclude that fewer cations are available for association with anions, reflecting slightly increased Li^+ solvation in P(EO-MO). Therefore, the higher density of available binding oxygens (p = 0.67) and increased polarity of the MO groups contribute to higher Li^+ solvation, while the availability of the second coordination shell and distorted binding geometries facilitate improved cation diffusivity in P(EO-MO).

To understand differences in anion diffusivity at a given reduced temperature, we considered anion–polymer interactions (Figure S21). RDF data were analyzed using distances between the nitrogen in $TFSI^-$ and either oxygen (Figure S21a) or carbon (Figure S21b) of the polymers. However, no significant variations were observed between the two compositions, suggesting minimal impacts on anion diffusivity resulting from anion–polymer interactions. Overall, the MD simulations provide insight into improved cation diffusivity in polyacetals via altered Li–polymer interactions, but do not provide insight into the lower D_F values for P(EO-MO).

Raman Spectroscopy. We employed Raman spectroscopy to further examine changes in local anion environments with respect to polymer composition. Vibrational bands in the 730–770 cm^{-1} range are well-known to correspond to the expansion–contraction mode of the $TFSI^-$ anion.[89,90] This mode has been thoroughly studied in ionic liquids,[91–93] polymer-based electrolytes,[94–96] and other LiTFSI-containing systems[90] and is commonly used as a measure of cation–anion clustering.

In concentrated electrolytes, anions are typically considered to be either "free" or "cation coordinated". Uncoordinated $TFSI^-$ (i.e., separated from Li^+ by solvent or polymer) is known to result in a Raman mode positioned at ~740 cm^{-1}. Shifts to higher wavenumbers occur with increasing coordination to Li^+ cations;[97] several discrete higher-wavenumber shifts have been assigned to distinct species.[89,98,99] However, at elevated temperatures, only one broad feature at ~745–750 cm^{-1} is typically observed,[100] ascribed to either contact ion pairs or larger clusters. In a contact ion pair, Li^+ is bound by two $TFSI^-$ oxygens from the same anion, giving a one-to-one ratio of anions and cations.[100] Clusters comprising one Li^+ and two or more anions are also known to exist,[91,100] such that the ratio of anions to cations is greater than one.

Raman spectra for PEO and the full polyacetal series at r = 0.08 were acquired at 90 °C, focusing on the $TFSI^-$ expansion–contraction mode from 730–770 cm^{-1} (Figure 6). For PEO, a singular feature at 739 cm^{-1} is observed, suggesting the vast majority of the $TFSI^-$ are not associating with cations. P(4EO-MO), P(3EO-MO) and P(2EO-MO) show a similar feature centered at 739 cm^{-1}, although a small shoulder shifted to higher wavenumbers (746 cm^{-1}) emerges. Therefore, these low-p electrolytes are dominated by free anions, with a small fraction of ion pairs. In addition to the "free" anion mode at 740–742 cm^{-1}, the most acetal-rich systems P(EO-MO) and P(EO-2MO) display a prominent feature at 746–748 cm^{-1}, indicative of contact ion pairs and ion aggregates. The appearance of both features in the spectra suggests the coexistence of free and coordinated $TFSI^-$ at similar concentrations in these two systems. The anion clustering observed by Raman spectroscopy appears independent of temperature (Figure S23), as also previously found by Edman in PEO-based electrolytes.[97] These distinct changes in anion environments as seen by Raman spectroscopy correlate well with the observed decreases in anion diffusivity at equivalent reduced temperature for P(EO-MO) and P(EO-2MO) (Figure 4b). We therefore attribute the slow diffusion of anions in these polyacetals to binding and/or clustering with cations to form larger, asymmetric ion clusters.

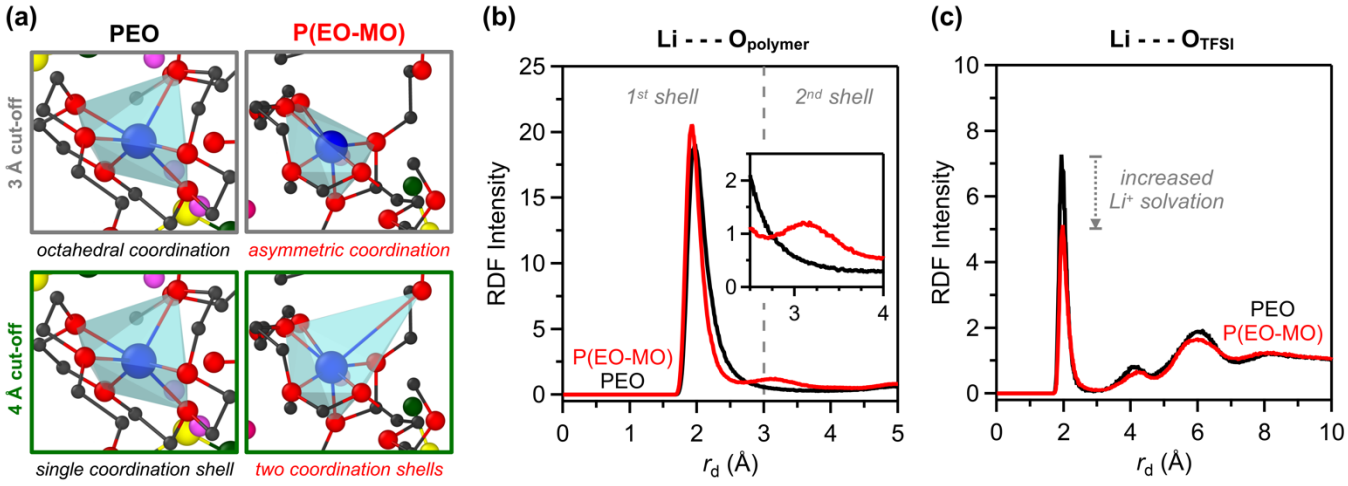

Figure 5. (a) Representative snapshots, (b) Li–$O_{polymer}$ radial distribution functions (RDFs), and (c) Li–O_{TFSI} RDFs from MD simulations of PEO/LiTFSI and P(EO-MO)/LiTFSI (at r = 0.08). The representative snapshots suggest that the local cation binding configuration for PEO is preferentially close to octahedral, while P(EO-MO) shows more asymmetric coordination on average. For both polymers, most Li–O coordination occurs within a 3 Å cut-off (first shell). In P(EO-MO), a second cationic coordination shell is observed from 2.5–4 Å, suggesting that additional proximal binding oxygens may enhance Li^+ diffusivity. P(EO-MO) shows a reduced intensity of the peak comprising short-range Li–TFSI interactions, indicating increased Li^+ solvation by P(EO-MO) compared to PEO. Colored spheres represent lithium (blue), oxygen (red), carbon (black), and sulfur (yellow). Hydrogen and fluorine atoms are omitted for clarity. The representative snapshots were produced using the OVITO software package.[88]

Together, MD simulations and Raman spectroscopy provide key insights into ion solvation and coordination in the acetal-rich polyacetals. RDF analysis reveals that P(EO-MO) has a smaller total number of Li–O_{TFSI} interactions (Figure 5c), corresponding to improved Li^+ solvation in the polymer due to both structural and chemical factors. This greater solvation leads to a larger proportion of available anions that bind to or cluster with non-polymer-bound Li^+, as demonstrated by Raman spectra (Figure 6). The greater number of large, anion-rich ion clusters in turn slows the anionic diffusivity (Figure 3b).

The molecular-level understanding of ion coordination and self-diffusion in polyacetals allows us to rationalize our recently reported electrochemical data.[41] . In that work, we observed lower ionic conductivities for the polyacetal electrolytes as compared to PEO. However, we identified that P(EO-MO) and P(EO-2MO) in fact possess higher efficacy values than PEO due to their relatively high current fractions. Using Raman spectroscopy and MD simulations in this work, we are able to elucidate that anion clustering in these systems is the likely origin of the high current fractions. Anion clustering is also confirmed by decreasing anion self-diffusion at equivalent reduced temperature in these two systems. All of these results indicate increased cationic diffusivity relative to the anion, as desired for high-efficacy polymer electrolyte systems.

An outstanding issue of polyacetal electrolytes remains their decreasing ionic conductivity with increasing *p*. Using MD simulations, we have confirmed that shorter O–CH_2–O bond distances in acetals do indeed distort Li^+ binding in these systems and provide proximal binding oxygens to aid in cation transport. However, the bound Li^+ in these systems likely forms interchain cross-links, leading to drastic increases in T_g with increasing acetal content. Analysis of Li^+ self-diffusion in comparison to PEO at a given reduced temperature allows us to decouple the effects of segmental motion, and in fact demonstrates improved Li diffusivity in polyacetals. This confirms that the origin of the decreasing conductivity is lower segmental motion related to the high T_g values of polyacetals. Therefore, the viability of polyacetal electrolytes as high-performance polymer

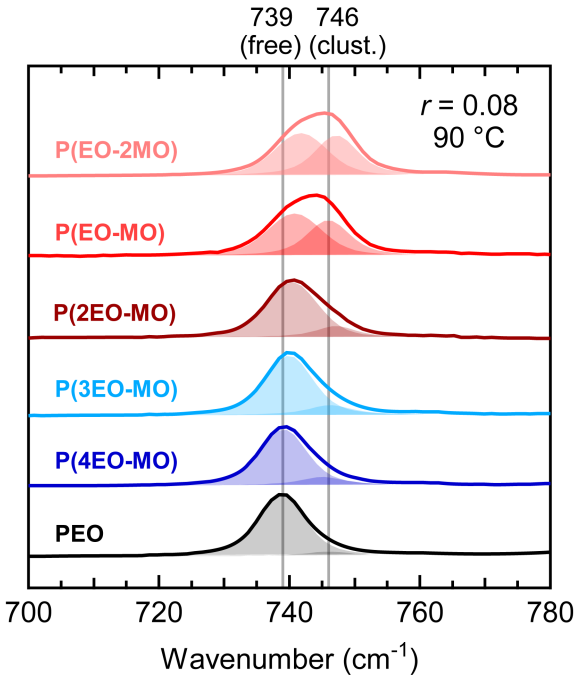

Figure 6. Raman spectra of the polymer electrolytes at r = 0.08 recorded at 90 °C, focusing on the peak associated with the $TFSI^-$ (anion) expansion–contraction mode, which is sensitive to the anion local environment and clustering interactions. Deconvolutions into "free" and clustered species are shown as filled peaks centered at 739 cm^{-1} and 746 cm^{-1}, respectively. (Note: P(2EO-MO) sample used was 55 kDa.)

electrolytes is dependent on reducing the T_g in order to access higher conductivities.

The structure–property relationships elucidated in this work also allow us to suggest explicit design principles for next-generation polymer electrolytes. We identify three practical targets: (1) increased cation diffusivity, (2) decreased anion diffusivity, and (3) lowered T_g. By increasing the diversity of cation coordination environments as well as the formation of anion-rich clusters, we have shown oxygen-rich polyacetals can meet the first two targets. The undesired increase in T_g, related to cation-induced "cross-linking" of chains, remains an outstanding problem. The next generation of polyacetal electrolytes will aim to minimize the salt-induced increase in T_g, while maintaining the advantages of high oxygen-to-carbon ratios.

Conclusions

In this work, we studied a systematic series of P(*x*EO-*y*MO) polyacetals with variable EO/MO ratios as potential and heretofore underexplored candidates for polymer electrolytes in Li-ion batteries. We first demonstrated the synthesis of thermally stable polyacetals via CROP of cyclic acetal monomers, highlighting the use of a highly soluble and readily removable NaOEtTMS quenching agent. Following electrolyte preparation with [LiTFSI] salt normalized to the number of oxygen binding groups, relative cation and anion self-diffusion coefficients were quantified using ^{7}Li and ^{19}F PFG-NMR at 90 °C, revealing decreasing anionic diffusivity with increasing acetal content of the polymer host. By normalizing diffusivity to account for differences in T_g, we

observe that all polyacetals exhibit faster cation self-diffusion than PEO at equivalent reduced temperature ($T - T_g$). While anion self-diffusion is similar to PEO for some materials, the most acetal-rich polymers P(EO-MO) and P(EO-2MO) demonstrate significantly slower anion diffusivity than PEO at similar reduced temperatures. MD simulations reveal that the shorter oxygen–oxygen distances (O–CH_2–O *vs.* O–CH_2–CH_2–O) in acetals induce geometrically distorted cation coordination environments, which provides a mechanism for increased cation diffusivity. Furthermore, P(EO-MO) shows a second Li–$O_{polymer}$ coordination shell from 3–4 Å; we anticipate these proximal oxygens aid in ion transport. The increased acetal content leads to a larger fraction of Li^+ associated with the polymer. In turn, improved Li^+ solvation is accompanied by anion clustering, as supported by Raman spectroscopy. Finally, the marked decrease in anionic self-diffusion at equivalent reduced temperature appears to be linked to formation of these clusters.

The faster cation and slower anion diffusivity observed herein provides an understanding of why polyacetals possess higher cationic current fractions. This work emphasizes that ion motion within polymer electrolytes can be tailored by modulating both cationic and anionic interactions by tuning the composition of the polymer host. By studying a systematic series of polymer electrolytes, we gained a fundamental mechanistic understanding of ion transport that supports the observed trends in both κ and ρ_+ in our prior work. In tandem, these studies reveal future design principles for improved polymer electrolyte performance and suggest the promise of polyacetal electrolytes for safe, high-performance LIBs.

ASSOCIATED CONTENT

The Supplementary Information is available free of charge at **DOI/XX**: Full synthetic procedures and characterization (NMR, GPC, TGA, DSC, and Raman); PFG-NMR definitions, parameters and full Stejskal-Tanner plots; technical details of MD simulations (**PDF**)

AUTHOR INFORMATION

Corresponding Authors

* (G.W.C.) Email: coates@cornell.edu
* (N.P.B.) Email: nbalsara@berkeley.edu
* (J.A.R.) Email: reimer@berkeley.edu

Author Contributions

† These authors contributed equally.

Notes

The authors have no competing interests or conflicts of interest to declare.

ACKNOWLEDGMENT

This work was fully supported by the Joint Center for Energy Storage Research (JCESR), an Energy Innovation Hub funded by the U.S. Department of Energy, Office of Science, Basic Energy Sciences. We thank the UC Berkeley College of Chemistry's NMR facility (CoC-NMR) for resources provided and the staff for their assistance. We also thank Dr. Ivan Keresztes at Cornell University for his help with the NMR analysis of P(EO-2MO). This work made use of the Cornell Center for Materials Research and the NMR Facility at Cornell University, which are supported by the NSF under awards DMR-1719875 and CHE-1531632, respectively. Raman experiments were performed at The Molecular Foundry, Lawrence Berkeley National Laboratory, and were supported by the Department of Energy, Office of Science, Office of Basic Energy Sciences, Scientific User Facilities Division of the U.S. Department of Energy under Contract No. DE-AC02-05CH11231. K.W.G. acknowledges funding from a National Defense and Science Engineering Graduate Fellowship. M.P.G. gratefully acknowledges the National Science Foundation for fellowship support under the National Science Foundation Graduate Research Fellowship Program.

REFERENCES

(1) Whittingham, M. S. Lithium Batteries and Cathode Materials. *Chem. Rev.* **2004**, *104*, 4271–4302.

(2) Dunn, B.; Kamath, H.; Tarascon, J.-M. Electrical Energy Storage for the Grid: A Battery of Choices. *Science* **2011**, *334*, 928–935.

(3) Etacheri, V.; Marom, R.; Elazari, R.; Salitra, G.; Aurbach, D. Challenges in the Development of Advanced Li-Ion Batteries: A Review. *Energy Environ. Sci.* **2011**, *4*, 3243–3262.

(4) Trahey, L.; Brushett, F. R.; Balsara, N. P.; Ceder, G.; Cheng, L.; Chiang, Y.-M.; Hahn, N. T.; Ingram, B. J.; Minteer, S. D.; Moore, J. S.; Mueller, K. T.; Nazar, L. F.; Persson, K. A.; Siegel, D. J.; Xu, K.; Zavadil, K. R.; Srinivasan, V.; Crabtree, G. W. Energy Storage Emerging: A Perspective from the Joint Center for Energy Storage Research. *Proc. Natl. Acad. Sci.* **2020**, *117*, 12550–12557.

(5) Xu, K. Nonaqueous Liquid Electrolytes for Lithium-Based Rechargeable Batteries. *Chem. Rev.* **2004**, *104*, 4303–4418.

(6) Wong, D. H. C.; Thelen, J. L.; Fu, Y.; Devaux, D.; Pandya, A. A.; Battaglia, V. S.; Balsara, N. P.; DeSimone, J. M. Nonflammable Perfluoropolyether-Based Electrolytes for Lithium Batteries. *Proc. Natl. Acad. Sci.* **2014**, *111*, 3327–3331.

(7) Mindemark, J.; Lacey, M. J.; Bowden, T.; Brandell, D. Beyond PEO—Alternative Host Materials for Li^+-Conducting Solid Polymer Electrolytes. *Prog. Polym. Sci.* **2018**, *81*, 114–143.

(8) Fenton, D. E.; Parker, J. M.; Wright, P. V. Complexes of Alkali Metal Ions with Poly(Ethylene Oxide). *Polymer* **1973**, *14*, 589.

(9) Armand, M. Polymer Solid Electrolytes - an Overview. *Solid State Ion.* **1983**, *9–10*, 745–754.

(10) Xue, Z.; He, D.; Xie, X. Poly(Ethylene Oxide)-Based Electrolytes for Lithium-Ion Batteries. *J. Mater. Chem. A* **2015**, *3*, 19218–19253.

(11) Di Noto, V.; Lavina, S.; Giffin, G. A.; Negro, E.; Scrosati, B. Polymer Electrolytes: Present, Past and Future. *Electrochimica Acta* **2011**, *57*, 4–13.

(12) Fergus, J. W. Ceramic and Polymeric Solid Electrolytes for Lithium-Ion Batteries. *J. Power Sources* **2010**, *195*, 4554–4569.

(13) Teran, A. A.; Tang, M. H.; Mullin, S. A.; Balsara, N. P. Effect of Molecular Weight on Conductivity of Polymer Electrolytes. *Solid State Ion.* **2011**, *203*, 18–21.

(14) Shriver, D. F.; Papke, B. L.; Ratner, M. A.; Dupon, R.; Wong, T.; Brodwin, M. Structure and Ion Transport in Polymer-Salt Complexes. *Solid State Ion.* **1981**, *5*, 83–88.

(15) Ratner, M. A.; Shriver, D. F. Ion Transport in Solvent-Free Polymers. *Chem. Rev.* **1988**, *88*, 109–124.

(16) Hayamizu, K.; Sugimoto, K.; Akiba, E.; Aihara, Y.; Bando, T.; Price, W. S. An NMR and Ionic Conductivity Study of Ion Dynamics in Liquid Poly(Ethylene Oxide)-Based Electrolytes Doped with $LiN(SO_2CF_3)_2$. *J. Phys. Chem. B* **2002**, *106*, 547–554.

(17) Gorecki, W.; Jeannin, M.; Belorizky, E.; Roux, C.; Armand, M. Physical Properties of Solid Polymer Electrolyte PEO(LiTFSI) Complexes. *J. Phys. Condens. Matter* **1995**, *7*, 6823–6832.

(18) Johansson, A.; Gogoll, A.; Tegenfeldt, J. Diffusion and Ionic Conductivity in $Li(CF_3SO_3)PEG_{10}$ and $LiN(CF_3SO_2)_2PEG_{10}$. *Polymer* **1996**, *37*, 1387–1393.

(19) Pesko, D. M.; Timachova, K.; Bhattacharya, R.; Smith, M. C.; Villaluenga, I.; Newman, J.; Balsara, N. P. Negative Transference Numbers in Poly(Ethylene Oxide)-Based Electrolytes. *J. Electrochem. Soc.* **2017**, *164*, E3569–E3575.

(20) Galluzzo, M. D.; Maslyn, J. A.; Shah, D. B.; Balsara, N. P. Ohm's Law for Ion Conduction in Lithium and beyond-Lithium Battery Electrolytes. *J. Chem. Phys.* **2019**, *151*, 020901.

(21) Diederichsen, K. M.; McShane, E. J.; McCloskey, B. D. Promising Routes to a High Li^+ Transference Number Electrolyte for Lithium Ion Batteries. *ACS Energy Lett.* **2017**, *2*, 2563–2575.

(22) Tominaga, Y. Ion-Conductive Polymer Electrolytes Based on Poly(Ethylene Carbonate) and Its Derivatives. *Polym. J.* **2017**, *49*, 291–299.

(23) Sun, B.; Mindemark, J.; Edström, K.; Brandell, D. Polycarbonate-Based Solid Polymer Electrolytes for Li-Ion Batteries. *Solid State Ion.* **2014**, *262*, 738–742.

(24) Hu, P.; Chai, J.; Duan, Y.; Liu, Z.; Cui, G.; Chen, L. Progress in Nitrile-Based Polymer Electrolytes for High Performance Lithium Batteries. *J. Mater. Chem. A* **2016**, *4*, 10070–10083.

(25) Forsyth, M.; Sun, J.; MacFarlane, D. R.; Hill, A. J. Compositional Dependence of Free Volume in $PAN/LiCF_3SO_3$ Polymer-in-Salt Electrolytes and the Effect on Ionic Conductivity. *J. Polym. Sci. Part B Polym. Phys.* **2000**, *38*, 341–350.

(26) Ali, F.; Forsyth, M.; Garcia, M. C.; Smith, M. E.; Strange, J. H. A ^7Li and ^{19}F NMR Relaxation Study of $LiCF_3SO_3$ in Plasticised Solid Polyether Electrolytes. *Solid State Nucl. Magn. Reson.* **1995**, *5*, 217–225.

(27) Babu, H. V.; Srinivas, B.; Muralidharan, K. Design of Polymers with an Intrinsic Disordered Framework for Li-Ion Conducting Solid Polymer Electrolytes. *Polymer* **2015**, *75*, 10–16.

(28) Hooper, R.; Lyons, L. J.; Mapes, M. K.; Schumacher, D.; Moline, D. A.; West, R. Highly Conductive Siloxane Polymers. *Macromolecules* **2001**, *34*, 931–936.

(29) Doyle, R. P.; Chen, X.; Macrae, M.; Srungavarapu, A.; Smith, L. J.; Gopinadhan, M.; Osuji, C. O.; Granados-Focil, S. Poly(Ethylenimine)-Based Polymer Blends as Single-Ion Lithium Conductors. *Macromolecules* **2014**, *47*, 3401–3408.

(30) Kawakami, Y.; Sugiura, T.; Yamashita, Y. Macrocyclic Formals. IV. Macrocyclic Formals as Complexing Agents. *Bull. Chem. Soc. Jpn.* **1978**, *51*, 3053–3056.

(31) Alamgir, M.; Moulton, R. D.; Abraham, K. M. Li^+-Conductive Polymer Electrolytes Derived from Poly(1,3-Dioxolane) and Polytetrahydrofuran. *Electrochimica Acta* **1991**, *36*, 773–782.

(32) Silva, R. A.; Goulart Silva, G.; Furtado, C. A.; Moreira, R. L.; Pimenta, M. A. Structure and Conductivity in Polydioxolane/$LiCF_3SO_3$ Electrolytes. *Electrochimica Acta* **2001**, *46*, 1493–1498.

(33) Goulart, G.; Sanchez, J.-Y.; Armand, M. Synthesis and Electrochemical Characterization of New Polymer Electrolytes Based on Dioxolane Homo and Co-Polymers. *Electrochimica Acta* **1992**, *37*, 1589–1592.

(34) Zhou, J.; Qian, T.; Liu, J.; Wang, M.; Zhang, L.; Yan, C. High-Safety All-Solid-State Lithium-Metal Battery with High-Ionic-Conductivity Thermoresponsive Solid Polymer Electrolyte. *Nano Lett.* **2019**, *19*, 3066–3073.

(35) Zhao, Q.; Liu, X.; Stalin, S.; Khan, K.; Archer, L. A. Solid-State Polymer Electrolytes with in-Built Fast Interfacial Transport for Secondary Lithium Batteries. *Nat. Energy* **2019**, *4*, 365–373.

(36) Khan, K.; Tu, Z.; Zhao, Q.; Zhao, C.; Archer, L. A. Synthesis and Properties of Poly-Ether/Ethylene Carbonate Electrolytes with High Oxidative Stability. *Chem. Mater.* **2019**, *31*, 8466–8472.

(37) Liu, F.-Q.; Wang, W.-P.; Yin, Y.-X.; Zhang, S.-F.; Shi, J.-L.; Wang, L.; Zhang, X.-D.; Zheng, Y.; Zhou, J.-J.; Li, L.; Guo, Y.-G. Upgrading Traditional Liquid Electrolyte via in Situ Gelation for Future Lithium Metal Batteries. *Sci. Adv.* **2018**, *4*, eaat5383.

(38) Nicholas, C. V.; Wilson, D. J.; Booth, C.; Giles, J. R. M. Improved Synthesis of Oxymethylene-Linked Poly(Oxyethylene). *Br. Polym. J.* **1988**, *20*, 289–292.

(39) Zheng, Q.; Pesko, D. M.; Savoie, B. M.; Timachova, K.; Hasan, A. L.; Smith, M. C.; Miller, T. F.; Coates, G. W.; Balsara, N. P. Optimizing Ion Transport in Polyether-Based Electrolytes for Lithium Batteries. *Macromolecules* **2018**, *51*, 2847–2858.

(40) Gao, K. W.; Loo, W. S.; Snyder, R. L.; Abel, B. A.; Choo, Y.; Lee, A.; Teixeira, S. C. M.; Garetz, B. A.; Coates, G. W.; Balsara, N. P. Miscible Polyether/Poly(Ether–Acetal) Electrolyte Blends. *Macromolecules* **2020**, *53*, 5728–5739.

(41) Snyder, R. L.; Choo, Y.; Gao, K. W.; Halat, D. M.; Abel, B. A.; Sundararaman, S.; Prendergast, D.; Reimer, J. A.; Balsara, N. P.; Coates, G. W. Improved Li^+ Transport in Polyacetal Electrolytes: Conductivity and Current Fraction in a Series of Polymers. *ACS Energy Lett.* **2021**, 1886–1891.

(42) Walderhaug, H.; Söderman, O.; Topgaard, D. Self-Diffusion in Polymer Systems Studied by Magnetic Field-Gradient Spin-Echo NMR Methods. *Prog. Nucl. Magn. Reson. Spectrosc.* **2010**, *56*, 406–425.

(43) Bhattacharja, S.; Smoot, S. W.; Whitmore, D. H. Cation and Anion Diffusion in the Amorphous Phase of the Polymer Electrolyte $(PEO)_8LiCF_3SO_3$. *Solid State Ion.* **1986**, *18–19*, 306–314.

(44) Boden, N.; Leng, S. A.; Ward, I. M. Ionic Conductivity and Diffusivity in Polyethylene Oxide/Electrolyte Solutions as Models for Polymer Electrolytes. *Solid State Ion.* **1991**, *45*, 261–270.

(45) Arumugam, S.; Shi, J.; Tunstall, D. P.; Vincent, C. A. Cation and Anion Diffusion Coefficients in a Solid Polymer Electrolyte Measured by Pulsed-Field-Gradient Nuclear Magnetic Resonance. *J. Phys. Condens. Matter* **1993**, *5*, 153–160.

(46) Hayamizu, K.; Aihara, Y.; Price, W. S. Correlating the NMR Self-Diffusion and Relaxation Measurements with Ionic Conductivity in Polymer Electrolytes Composed of Cross-Linked Poly(Ethylene Oxide-Propylene Oxide) Doped with $LiN(SO_2CF_3)_2$. *J. Chem. Phys.* **2000**, *113*, 4785–4793.

(47) Gresham, W. F.; Bell, C. D. Preparation of Polydioxolane. US 2394910, February 12, 1946.

(48) Gresham, W. F.; Bell, C. D. Preparation of Dioxolane Polymers. US 2395265, February 19, 1946.

(49) Hill, J. W.; Carothers, W. H. Cyclic and Polymeric Formals. *J. Am. Chem. Soc.* **1935**, *57*, 925–928.

(50) Albrecht, K.; Fleischer, D.; Kane, A.; Rentsch, C.; Thi, Q. V. T.; Yamaguchi, H.; Schulz, R. C. Polymerization of Macrocyclic Formals. *Makromol. Chem.* **1977**, *178*, 881–883.

(51) Kawakami, Y.; Suzuki, J.; Yamashita, Y. Macrocyclic Formals. V. Cationic Polymerization of 1,3,6,9,12-Pentaoxacyclotetradecane. *Polym. J.* **1977**, *9*, 519–524.

(52) Gresham, W. F.; Bell, C. D. Trioxepane and Its Polymers. US 2475610, July 12, 1949.

(53) Penczek, S. Cationic Ring-Opening Polymerization (CROP) Major Mechanistic Phenomena. *J. Polym. Sci. Part Polym. Chem.* **2000**, *38*, 1919–1933.

(54) Gong, M. S.; Hall, H. K. Trialkylsilyl Triflates, Novel Initiators for Cationic Polymerization. *Macromolecules* **1986**, *19*, 3011–3012.

(55) Neitzel, A. E.; Barreda, L.; Trotta, J. T.; Fahnhorst, G. W.; Haversang, T. J.; Hoye, T. R.; Fors, B. P.; Hillmyer, M. A. Hydrolytically-Degradable Homo- and Copolymers of a Strained Exocyclic Hemiacetal Ester. *Polym. Chem.* **2019**, *10*, 4573–4583.

(56) Yamashita, Y.; Mayumi, J.; Kawakami, Y.; Ito, K. Ring-Chain Equilibrium of Macrocyclic Formals. *Macromolecules* **1980**, *13*, 1075–1080.

(57) Rentsch, C.; Schulz, R. C. Cyclic Oligomers Formed during the Polymerization of 1,3,6,9-Tetraoxacycloundecane. *Makromol. Chem.* **1977**, *178*, 2535–2544.

(58) Kawakami, Y.; Yamashita, Y. Macrocyclic Formals. II. The Effect of Initiators and Solvents on the Two Stage Polymerization of 1, 3, 6, 9-Tetraoxa-Cycloundecane. *Polym. J.* **1977**, *9*, 227–230.

(59) Kawakami, Y.; Yamashita, Y. Macrocyclic Formals. 3. Two-Stage Polymerization of 1,3-Dioxacycloalkanes. *Macromolecules* **1977**, *10*, 837–839.

(60) Xu, B.; Lillya, C. P.; Chien, J. C. W. Cationic Polymerizations of 1,3,6-Trioxocane and 2-Butyl-1,3,6-Trioxocane. *Macromolecules* **1987**, *20*, 1445–1450.

(61) Fleischer, D.; Schulz, R. C. NMR-Untersuchungen an Polyacetalen, 4. Sequenzanalyses von Homo- und Copolymeren des 1,3,5-Trioxepans. *Makromol. Chem.* **1975**, *1*, 235–247.

(62) Timachova, K.; Watanabe, H.; Balsara, N. P. Effect of Molecular Weight and Salt Concentration on Ion Transport and the Transference Number in Polymer Electrolytes. *Macromolecules* **2015**, *48*, 7882–7888.

(63) Hayamizu, K.; Akiba, E.; Bando, T.; Aihara, Y. ^{1}H, ^{7}Li, and ^{19}F Nuclear Magnetic Resonance and Ionic Conductivity Studies for Liquid Electrolytes Composed of Glymes and Polyetheneglycol Dimethyl Ethers of $CH_3O(CH_2CH_2O)_nCH_3$ (n=3–50) Doped with $LiN(SO_2CF_3)_2$. *J. Chem. Phys.* **2002**, *117*, 5929–5939.

(64) Orädd, G.; Edman, L.; Ferry, A. Diffusion: A Comparison between Liquid and Solid Polymer LiTFSI Electrolytes. *Solid State Ion.* **2002**, *152–153*, 131–136.

(65) Cotts, R. M.; Hoch, M. J. R.; Sun, T.; Markert, J. T. Pulsed Field Gradient Stimulated Echo Methods for Improved NMR Diffusion Measurements in Heterogeneous Systems. *J. Magn. Reson.* **1989**, *83*, 252–266.

(66) Witherspoon, V. A Magnetic Resonance Perspective of Adsorbates Motion in Metal Organic Frameworks. PhD Thesis, University of California, Berkeley, 2017.

(67) Friedemann, K.; Stallmach, F.; Kärger, J. NMR Diffusion and Relaxation Studies during Cement Hydration—A Non-Destructive Approach for Clarification of the Mechanism of Internal Post Curing of Cementitious Materials. *Cem. Concr. Res.* **2006**, *36*, 817–826.

(68) Gorecki, W.; Andreani, R.; Berthier, C.; Armand, M.; Mali, M.; Roos, J.; Brinkmann, D. NMR, DSC, and Conductivity Study of a Poly(Ethylene Oxide) Complex Electrolyte : $PEO(LiClO_4)_x$. *Solid State Ion.* **1986**, *18–19*, 295–299.

(69) Aihara, Y.; Bando, T.; Nakagawa, H.; Yoshida, H.; Hayamizu, K.; Akiba, E.; Price, W. S. Ion Transport Properties of Six Lithium Salts Dissolved in γ-Butyrolactone Studied by Self-Diffusion and Ionic Conductivity Measurements. *J. Electrochem. Soc.* **2004**, *151*, A119–A122.

(70) Cameron, G. G.; Ingram, M. D.; Harvie, J. L. Ion Transport in Polymer Electrolytes. *Faraday Discuss. Chem. Soc.* **1989**, *88*, 55–63.

(71) Balsara, N. P.; Newman, J. Relationship between Steady-State Current in Symmetric Cells and Transference Number of Electrolytes Comprising Univalent and Multivalent Ions. *J. Electrochem. Soc.* **2015**, *162*, A2720–A2722.

(72) Shah, D. B.; Nguyen, H. Q.; Grundy, L. S.; Olson, K. R.; Mecham, S. J.; DeSimone, J. M.; Balsara, N. P. Difference between Approximate and Rigorously Measured Transference Numbers in Fluorinated Electrolytes. *Phys. Chem. Chem. Phys.* **2019**, *21*, 7857–7866.

(73) D'Angelo, A. J.; Panzer, M. J. Enhanced Lithium Ion Transport in Poly(Ethylene Glycol) Diacrylate-Supported Solvate Ionogel Electrolytes via Chemically Cross-Linked Ethylene Oxide Pathways. *J. Phys. Chem. B* **2017**, *121*, 890–895.

(74) Orädd, G.; Furlani, M.; Ferry, A. Diffusion and Dielectric Studies of the System PPO4000–$NH_4CF_3SO_3$. *Solid State Ion.* **2000**, *136–137*, 457–461.

(75) Gorecki, W.; Roux, C.; Clémancey, M.; Armand, M.; Belorizky, E. NMR and Conductivity Study of Polymer Electrolytes in the Imide Family: $P(EO)/Li[N(SO_2C_nF_{2n+1})(SO_2C_mF_{2m+1})]$. *ChemPhysChem* **2002**, *3*, 620–625.

(76) Diederichsen, K. M.; Fong, K. D.; Terrell, R. C.; Persson, K. A.; McCloskey, B. D. Investigation of Solvent Type and Salt Addition in High Transference Number Nonaqueous Polyelectrolyte Solutions for Lithium Ion Batteries. *Macromolecules* **2018**, *51*, 8761–8771.

(77) Gouverneur, M.; Schmidt, F.; Schönhoff, M. Negative Effective Li Transference Numbers in Li Salt/Ionic Liquid Mixtures: Does Li Drift in the "Wrong" Direction? *Phys. Chem. Chem. Phys.* **2018**, *20*, 7470–7478.

(78) Grundy, L. S.; Shah, D. B.; Nguyen, H. Q.; Diederichsen, K. M.; Celik, H.; DeSimone, J. M.; McCloskey, B. D.; Balsara, N. P. Impact of Frictional Interactions on Conductivity, Diffusion, and Transference Number in Ether- and Perfluoroether-Based Electrolytes. *J. Electrochem. Soc.* **2020**, *167*, 120540.

(79) Bruce, P. G.; Vincent, C. A. Steady State Current Flow in Solid Binary Electrolyte Cells. *J. Electroanal. Chem. Interfacial Electrochem.* **1987**, *225*, 1–17.

(80) Evans, J.; Vincent, C. A.; Bruce, P. G. Electrochemical Measurement of Transference Numbers in Polymer Electrolytes. *Polymer* **1987**, *28*, 2324–2328.

(81) Borodin, O.; Smith, G. D. Mechanism of Ion Transport in Amorphous Poly(Ethylene Oxide)/LiTFSI from Molecular Dynamics Simulations. *Macromolecules* **2006**, *39*, 1620–1629.

(82) Diddens, D.; Heuer, A.; Borodin, O. Understanding the Lithium Transport within a Rouse-Based Model for a PEO/LiTFSI Polymer Electrolyte. *Macromolecules* **2010**, *43*, 2028–2036.

(83) Lascaud, S.; Perrier, M.; Vallee, A.; Besner, S.; Prud'homme, J.; Armand, M. Phase Diagrams and Conductivity Behavior of Poly(Ethylene Oxide)-Molten Salt Rubbery Electrolytes. *Macromolecules* **1994**, *27*, 7469–7477.

(84) Zhang, S.; Dou, S.; Colby, R. H.; Runt, J. Glass Transition and Ionic Conduction in Plasticized and Doped Ionomers. *J. Non-Cryst. Solids* **2005**, *351*, 2825–2830.

(85) Diederichsen, K. M.; Buss, H. G.; McCloskey, B. D. The Compensation Effect in the Vogel–Tammann–Fulcher (VTF) Equation for Polymer-Based Electrolytes. *Macromolecules* **2017**, *50*, 3831–3840.

(86) Borodin, O.; Smith, G. D. Molecular Dynamics Simulations of Poly(Ethylene Oxide)/LiI Melts. 1. Structural and Conformational Properties. *Macromolecules* **1998**, *31*, 8396–8406.

(87) Wang, Y.; Richards, W. D.; Ong, S. P.; Miara, L. J.; Kim, J. C.; Mo, Y.; Ceder, G. Design Principles for Solid-State Lithium Superionic Conductors. *Nat. Mater.* **2015**, *14*, 1026–1031.

(88) Stukowski, A. Visualization and Analysis of Atomistic Simulation Data with OVITO–the Open Visualization Tool. *Model. Simul. Mater. Sci. Eng.* **2009**, *18*, 015012.

(89) Bakker, A.; Gejji, S.; Lindgren, J.; Hermansson, K.; Probst, M. M. Contact Ion Pair Formation and Ether Oxygen Coordination in the Polymer Electrolytes $M[N(CF_3SO_2)_2]_2PEO_n$ for M = Mg, Ca, Sr and Ba. *Polymer* **1995**, *36*, 4371–4378.

(90) Brouillette, D.; Irish, D. E.; Taylor, N. J.; Perron, G.; Odziemkowski, M.; Desnoyers, J. E. Stable Solvates in Solution of Lithium Bis(Trifluoromethylsulfone)Imide in Glymes and Other Aprotic Solvents: Phase Diagrams, Crystallography and Raman Spectroscopy. *Phys. Chem. Chem. Phys.* **2002**, *4*, 6063–6071.

(91) Angenendt, K.; Johansson, P. Ionic Liquid Based Lithium Battery Electrolytes: Charge Carriers and Interactions Derived by Density Functional Theory Calculations. *J. Phys. Chem. B* **2011**, *115*, 7808–7813.

(92) Monti, D.; Jónsson, E.; Palacín, M. R.; Johansson, P. Ionic Liquid Based Electrolytes for Sodium-Ion Batteries: Na^+ Solvation and Ionic Conductivity. *J. Power Sources* **2014**, *245*, 630–636.

(93) Nürnberg, P.; Lozinskaya, E. I.; Shaplov, A. S.; Schönhoff, M. Li Coordination of a Novel Asymmetric Anion in Ionic Liquid-in-Li Salt Electrolytes. *J. Phys. Chem. B* **2020**, *124*, 861–870.

(94) Bakker, A.; Lindgren, J.; Hermansson, K. Polymer Electrolytes Based on Triblock-Copoly(Oxyethylene/Oxypropylene/Oxyethylene) Systems. *Polymer* **1996**, *37*, 1871–1878.

(95) Ferry, A.; Doeff, M. M.; De Jonghe, L. C. Transport Property and Raman Spectroscopic Studies of the Polymer Electrolyte System $P(EO)_n$-NaTFSI. *J. Electrochem. Soc.* **1998**, *145*, 1586.

(96) Rey, I.; Lassègues, J. C.; Grondin, J.; Servant, L. Infrared and Raman Study of the PEO-LiTFSI Polymer Electrolyte. *Electrochimica Acta* **1998**, *43*, 1505–1510.

(97) Edman, L. Ion Association and Ion Solvation Effects at the Crystalline–Amorphous Phase Transition in PEO–LiTFSI. *J. Phys. Chem. B* **2000**, *104*, 7254–7258.

(98) Arnaud, R.; Benrabah, D.; Sanchez, J.-Y. Theoretical Study of CF_3SO_3Li, $(CF_3SO_2)_2NLi$, and $(CF_3SO_2)_2CHLi$ Ion Pairs. *J. Phys. Chem.* **1996**, *100*, 10882–10891.

(99) Lassègues, J.-C.; Grondin, J.; Aupetit, C.; Johansson, P. Spectroscopic Identification of the Lithium Ion Transporting Species in LiTFSI-Doped Ionic Liquids. *J. Phys. Chem. A* **2009**, *113*, 305–314.

(100) Zhou, Q.; Boyle, P. D.; Malpezzi, L.; Mele, A.; Shin, J.-H.; Passerini, S.; Henderson, W. A. Phase Behavior of Ionic Liquid–LiX Mixtures: Pyrrolidinium Cations and $TFSI^-$ Anions – Linking Structure to Transport Properties. *Chem. Mater.* **2011**, *23*, 4331–4337.

Insert Table of Contents artwork here